Separation and Purification Technology 270 (2021) 118818

Contents lists available at ScienceDirect

Separation and Purification Technology

journal homepage: www.elsevier.com/locate/seppur

Mechanism of permeance enhancement in mixed-matrix reverse osmosis membranes incorporated with graphene and its oxides

Guxu Wang, Xin Zhang, Mingjie Wei *, Yong Wang

State Key Laboratory of Materials-Oriented Chemical Engineering, and College of Chemical Engineering, Nanjing Tech University, Nanjing 211816, Jiangsu, PR China

ARTICLE INFO

Keywords:
Transport mechanism
Mixed-matrix membrane
Reverse osmosis
Thin-film nanocomposite
Graphene oxides

ABSTRACT

Fabricating mixed-matrix reverse osmosis (RO) membranes via incorporating nanocomposites is a promising strategy to enhance permeance performance without sacrificing the ion rejection. To better design such mixed-matrix membranes (MMMs), the transport mechanism of water molecules through them is urgently desired. Compared to the stiff inorganic nanoparticles, the flexible graphene (Gr) and its oxides (GO) attract much attention due to their better compatibility with aromatic polyamide (PA) matrix. In this work, nonequilibrium molecular dynamics simulations of water passing through highly cross-linked PA membranes, Gr/PA and GO/PA MMMs are performed to reveal the transport mechanism. The simulation results show that the MMMs exhibit higher permeance compared to the pure PA membranes. After analyzing the transport details of water molecules, we discovered that the permeance enhancement for two types of MMMs result from distinct factors. While the Gr/PA MMMs have lower interior transport resistance because of the hydrophobic nature of Gr, the permeance enhancement of GO/PA MMMs should be attributed to the higher solubility of water molecules into MMMs. Therefore, a proper hydrophilicity of RO membrane, which has lower interior transport resistance while having higher solubility, is expected for the optimized performance.

1. Introduction

While the world population and industrialization grows rapidly, there is an ongoing rising demand for fresh water. Its safety and availability are inextricably linked to human health, energy production, and economic development [1]. Obtaining fresh water from seawater plays a more and more important role as most developed cities and industrial towns are offshore. Among all technologies, the reverse osmosis (RO) technology dominates the newly built-up desalination plants [2,3], because of its energy efficiency [4] compared to some of the thermal desalination technologies including multi-effect distillation, multi-stage flash and vapor compression distillation, as well as others like the emerging technology of capacitive deionization [5].

As the key element of RO technology, RO membranes determine the performance of RO technology, including salt rejection and water permeance. Although the current commercial thin-film composite RO membranes perform the salt rejection of higher than 99.5%, the flux is still unsatisfactory compared to the demand of life, industry and agriculture. Therefore, enhancing the permeance of RO membranes draws the most researchers' attention. While the RO membranes consist of a three-layered structure, the skin layer of dense polyamide dominates the transport resistance of water molecules, and therefore, the attention is mainly paid to this layer. The common consideration of reducing the transport resistance is to decline the thickness of the skin layer. Jiang et al. prepare the ultrathin PA nanofilm and the prepared thin-film composite (TFC) membranes exhibit proportional increase of permeance [6]. Another novel consideration is to build up nanovesicles with uniform structure [7] or with nanoparticles as a sacrificial templating material [8], which will evidently increase the membrane surface area. Unfortunately, the above two methods cannot promote the flux of membranes without the sacrifice of salt rejection.

The mixed-matrix membranes (MMMs) are expected to be an alternative way to promote the flux of RO membranes. Jeong et al. successfully incorporate the zeolite nanoparticles inside the PA skin layer of TFC RO membranes [9]. Such-prepared membranes are also called thin-film nanocomposite membranes, as they inherit the advantage of the ultra-thin skin layer of TFC RO membranes while keeping nanoparticles inside the skin layers [10]. Furthermore, the prepared MMMs were applied in industrial applications soon by the company of NanoH_2O and were applied in the industrial desalination. Moreover, by incorporating

* Corresponding author.
E-mail address: mj.wei@njtech.edu.cn (M. Wei).

https://doi.org/10.1016/j.seppur.2021.118818
Received 3 February 2021; Received in revised form 7 April 2021; Accepted 19 April 2021
Available online 23 April 2021

aquaporins into RO membranes, the company of Aquaporin prepared another MMMs and soon applied them into industrial application [11]. Inspired by the success of above mentioned two kinds of MMMs, several researchers make great efforts to incorporate other nanoparticles into the skin layer of RO membranes. For example, with metal–organic framework (ZIF-8) nanoparticles incorporated into MMMs, their water permeance was increased by 43.8% [12]. Due to the good compatibility of carbon nanotubes (CNTs) with PA matrix, the CNTs are commonly incorporated into MMMs, which exhibit promoted water permeance [13–16]. The nonporous TiO_2 nanoparticles are also incorporated, and the prepared MMMs exhibit excellent anti-bacterial performance [17], similar findings are also revealed by Gai et al from their MMMs incorporated with carbon quantum dots [18,19].

Although there are several published works of RO MMMs and almost all of these membranes exhibit the promotion of permeance, the mechanism of such promotion is still controversial. There are usually two points of view: 1, the instinct nanopores of nanoparticles provide more channels for the transport of water molecules [16,20–22]; 2, the adding of nanoparticles improves the hydrophilicity of MMMs [23–25]. Our previous work reveals that the nanopores of covalent organic frameworks nanoparticles, which were added into polyamide (PA) membranes, could not help to promote the water flux, because the nanopore would be blocked at the entrance and exit by PA chains [26]. Interestingly, the incompatibility of such nanoparticles, which is much stiff compared to PA matrix, will form an incompatibility region at their interfaces. In that region, the transport of water is higher than that in PA matrix, and consequently promotes the permeance of MMMs. It is a pity that the incompatibility will result in a severe problem of the agglomeration of nanoparticles while preparing the membranes. Hence, adding the nanoparticles that are compatible with PA, even without pores, will be more practical for experimental preparation.

In this work, we select graphene and its oxide as nano-additives, which have similar chemical structures with aromatic PA matrix, to build up the mixed-matrix RO membranes. Using non-equilibrium molecular dynamics (NEMD) simulations, the permeance mechanism of water molecules through RO MMMs can be revealed. One of the advantages of NEMD simulations is to investigate the complex transport phenomena by separate factors. By applying two sets of MMMs, the swelling and nonswelling, we obtain the contributions of solution and diffusion in the solution-diffusion model of RO membranes. The mechanisms of permeance promotion of Gr/PA and GO/PA MMMs are respectively disclosed.

2. Simulation details

2.1. Modeling of the dry pure PA membrane

The commercial RO membranes are commonly synthesized by interfacial polymerization of trimesoyl chloride (TMC) and phenylenediamine (MPD) monomers (see Fig. 1) and the prepared PA skin layer has a highly cross-linked molecular structure. In order to model such a highly cross-linked molecular structure, we followed the work of Ding et al. [27], modeling the crosslinking of PA by two steps: the construction of linear PA chains and the crosslinking of linear chains by adding MPD monomers. By this method, the degree of crosslinking can be easily controlled by tuning the number of additional MPD monomers inserted in the simulation. Five PA chains, composed of 30 TMC monomers for each, were first built up and then put into a simulation box. Since we constructed the PA membranes rather than the bulk materials, we applied periodic boundary conditions (PBCs) only in x and y direction, so that the membrane surfaces could form in z direction. Afterward, a standard minimization protocol was used to minimize the energy structure via a Polak–Ribiere algorithm. As indicated in the work of Ding et al. [27], the existence of water molecules would not influence the interactions between MPD monomers and polyamide chains, we performed the crosslinking process without external reservoirs.

In order to construct the highly cross-linked PA membranes, 50 MPD molecules were then inserted into simulation box, followed by a 2-ns equilibrium molecular dynamics (EMD) simulation in the isothermal-isobaric ensemble (NPT). To accelerate the contact of MPD with carboxyl groups (COOH) in the PA chains, the temperature was set to 600 K while pressure being 1 bar and the interaction between N atoms in MPD and double-bonded O atoms in the COOH group was 100 times enhanced.

After the 2-ns simulation, the carbon–nitrogen (N-O) radial distribution function (RDF) was calculated between nitrogen atoms in MPD molecules and the oxygen atoms of COOH groups of PA chains. Based on the RDF results (shown in Fig. S3), we determined the most probable distance between these oxygen and nitrogen atoms, d_p, as 0.5 nm, which was set as the threshold for defining the formation of amide bonds. If the distance between the carbon and nitrogen atoms was smaller than d_p, we manually added a covalent bond between these two atoms and removed the rest two hydrogen and one oxygen atoms by our own codes (see illustration in Fig. S1a). We repeated this procedure several times and the 50 MPD monomers would be cross-linked to the PA chains. The target crosslinking degree of 88.8%, which was calculated by the methods proposed by Kolev and Freger [28], as

$$I = \frac{n_N}{n_N + n_{COOH}} \times 100\% \quad (1)$$

where n_N and n_{COOH} are the number of nitrogen atoms and that of COOH groups in the membrane, respectively. Although the target crosslinking degree is higher than those from other simulation work [29,30], it is in accordance with the experimental data, which was measured to be 60%-100% by either X-ray photoelectron spectrometry [31–33] and Rutherford backscattering spectrometry [32,34].

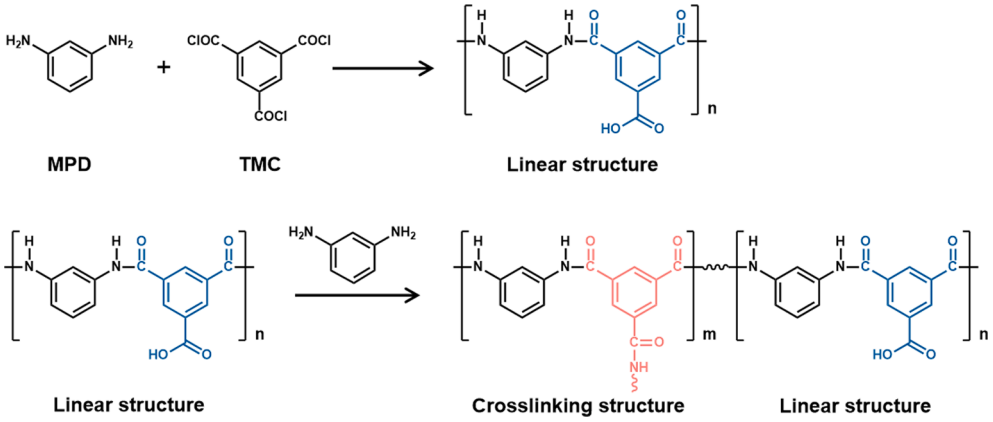

Fig. 1. Illustration of chemical structure when building up the cross-linked PA.

An EMD simulation was then performed for a few nanoseconds in order to relax the cross-linked structure and to get a correct membrane density. Finally, we obtained a dry PA membrane with the density of 1.06 g cm^{-3} and the final dimensions of the simulation box were $L_x = L_y = 3.63$ nm and $L_z = 5.3$ nm. It is worth noting that the PBCs exist only in x and y direction during all above simulations and consequently the surfaces for PA at z direction always remain. Moreover, we placed two solid and frozen plates at the surfaces of membranes, so that the membranes thickness can be restricted as 5.3 nm for all cases.

2.2. Modeling of the hydrated pure PA membrane

Two water reservoirs were added to the simulation box, outside the obtained dry PA membrane at z direction. In order to push water molecules into dry PA membranes, two flexible graphene walls acting as pistons were added on each side of the membrane/reservoir system along z direction (Fig. 3). Simulations were carried out in the canonical ensemble (NVT) and an external force generating a pressure of 1 bar was applied on each graphene wall.

The membrane hydration process would also be divided into two parts: non-swelling hydration and swelling hydration. Swelling hydration is well understood as free swelling without any treatment of the membrane, which is similar to the experimental situations. Non-swelling hydration indicates that swelling is not allowed to occur at the interface between the membrane and the water reservoirs during hydration, but water molecules are simply allowed to enter the free volume of the membrane. In order to achieve this goal, part of membrane atoms at the interface between the membrane and the water reservoirs were restrained in the z-direction by a force constant of 10 kJ mol^{-1} nm^{-2}, but could move in the x and y direction accounting for membrane flexibility, which was similar to Liu et al. [35]. Herein, we selected the nitrogen in amide groups to be constrained, so as to prevent the membrane surface from swelling. The constrained nitrogen accounts for about 0.87% of the total membrane atoms, and will thus take very little effect on the PA movement. It is worth noting that this method of membrane hydration is extremely slow. Therefore, an 8-step protocol [35], similar to the annealing process in the experiment, was adopted in this work to accelerate the hydration process of the non-swollen membrane, which is introduced in details in Table S1. Moreover, the calculation time was saved by increasing the temperature, which was set to 400 K, to enhance the motion of the water molecules and the membrane. After three cycles of the 8-step protocol, the dry PA membrane was completely hydrated without swelling. In cases of the swollen membrane, an additional 40-ns simulation in a room condition (300 K, 1 bar) was carried out, in which the constrained atoms were released.

2.3. Modeling the mixed-matrix membranes

In this work, we selected a piece of nanosheet of graphene (Gr) and graphene oxides (GO) as the additive, whose dimensions are $L_x = 2.0$ nm, $L_z = 2.5$ nm. One nanosheet of Gr or GO was firstly placed in the center of the simulation box while the normal direction of sheets was alone y direction. The nanosheets in PA would be placed parallel to flow direction (z) consequently, which will not significantly hinder the flow due to position blocking. 5 PA chains were then added into simulation box, followed by the subsequent procedure mentioned in section 2.1. Moreover, in order to prevent the linear polyamide from overlapping or getting too closer to the nanoparticles, a standard minimization protocol was used to minimize the energy structure to relax the system. In order to keep the thickness of MMMs the same as that of pure PA membranes, the thickness of MMMs was restricted to 5.3 nm. Therefore, 4-ns simulation was performed in NPT ensemble only in the xy direction at the room condition (300 K, 1 bar) when we constructed the dry cross-linked MMMs and L_z was kept at 5.3 nm. The final structure of the dry membranes is shown in Fig. 2 b and c for Gr/PA and GO/PA MMMs, respectively. The hydration process is the same to that of pure PA membranes as introduced in section 2.2.

Following the Lerf-Klinowski model [36,37], we consider both hydroxyl and epoxy groups for GO nanosheets, which represents typical outcomes from the standard oxidation process. The epoxy and hydroxyl groups were located on the basal plane (both sides), and the carboxyl groups were attached to the carbon atoms on the edge. The distribution of oxidized groups in GO was set to be either random or regular in our models. The value of the oxygen content, c, varies depending on the degree of oxidation in the preparation processes [38]. In our simulation, we selected a typical value of c at ~ 20%, which is close to most experimental data [39,40]. A typical composition of GO, $C_{10}O_1(OH)_1(COOH)_{0.5}$ was selected in this work.

2.4. Details of NEMD simulations

As there were two sets of hydrated membranes, swollen and non-swollen, we measured the permeance of them by distinct methods. For the swollen membranes, salt ions of sodium chloride with a concentration of 0.6 mol L^{-1} was added to the left-side water reservoir to simulate seawater (Fig. 3). As the existing commercial thin-film composite (TFC) RO membranes perform the salt rejection of higher than 99.5%, it is difficult for ions to penetrate into the PA matrix. Therefore, in the cases of the non-swollen membrane, we paid more attention to the pure water

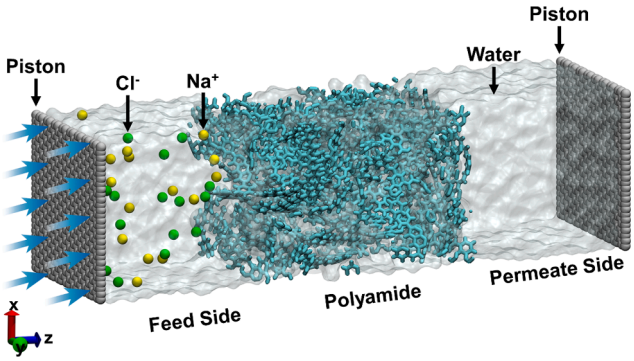

Fig. 3. Snapshot of nonequilibrium molecular dynamics of reverse osmosis process through the constructed hydrated membranes.

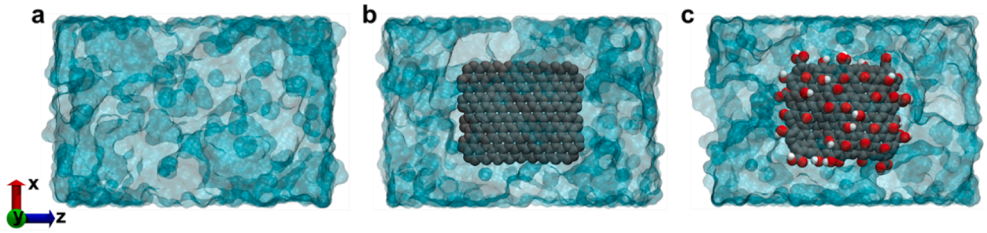

Fig. 2. Snapshot of the constructed dry cross-linked membranes. (a) pure PA membranes, (b) graphene/PA and (c) graphene oxide/PA mixed-matrix membranes. Transparent cyan represents dry PA membrane, while gray, red and white represents, graphene sheets, oxygen and hydrogen atoms of graphene oxide, respectively.

permeance rather than that of seawater and only performed the pure water flux measurements for non-swollen membranes. In this work, the external force, F, along the z/-z direction was applied to each atom of the two pistons to obtain the desired pressures on the pistons. The relationship is described as

$$P = \frac{nF}{A} \tag{2}$$

where P is the desired pressure drop on the piston, A is the area of the piston, and n represents the atom number of each piston. The applied ΔP, denoted as the pressure drop between upper and lower pistons, was 500 MPa. Such high ΔP is commonly used in NEMD to reduce the thermal noise and enhance signal/noise ratio within the simulation time scale of nanoseconds [41–43,16–20]. The temperature of the PA and water molecules was regulated using a canonical ensemble (NVT) at 300 K. At the same time, to prevent PA from flowing with water molecules, a few PA atoms were pinned at certain positions [44], similar to the non-swelling hydration. Each simulation was performed for 80 ns with a time step of 1 fs. The first 20 ns simulation was allowed to reach a steady state, not for further analysis. Data from the remaining 60 ns simulation was collected to analyze the structural and dynamics properties of the water molecules and membranes by the self-compiled codes.

2.5. Molecular interactions and other simulation details

The interactions of all atoms were represented by the Lennard-Jones (LJ) and Columbic potentials. The standard SPC/E [45] model was used for the water molecules. To decrease the high-frequency vibrations and reduce the simulation time, the SHAKE algorithm was used to constrain the bonds and angles of the water molecules. LJ parameters for the atoms of PA are obtained from the Amber force field [46], which is successfully applied in other PA simulations [27,44,47]. The graphene and GO were modeled by means of the OPLS-AA force field [48], because this type of force field will well the motion and twist of nanosheets of graphene and its oxides. The Lorentz-Berthelot mixing rule was adopted for all pair-wise LJ terms. The cut-off distances of 1.0 and 1.2 nm were used to calculate the LJ and Coulombic potentials, respectively. Lennard–Jones parameters of two pistons on either side of the water reservoirs were consistent with those of graphene. All simulations were carried out using the Large-scale Atomic/Molecular Massively Parallel Simulator (LAMMPS) package [49].

3. Results and discussions

The advantage of NEMD simulations is utilized to obtain the transport performance of membranes while observing the molecular details of membranes and fluid. In this part, the transport performance of pure PA, Gr/PA and GO/PA membranes are firstly introduced. The molecular details are then revealed followed by the discussions on transport mechanism for MMMs.

3.1. Apparent water permeance

In order to compare the performance of the new membranes, the permeability of them is most concerned. Since the permeability is related to the membrane thickness, the membrane thickness should be kept the same when we try to compare the permeability of distinct membranes. As introduced in section 2.3, all constructed hydrated membranes are kept the same in thickness, especially in the cases of non-swollen those. In the cases of swollen membranes, the main thicknesses of distinct membranes are almost the same, and the swelling occurs usually near the interfacial region due to the highly cross-linked structure.

The permeances of pure PA, Gr/PA and GO/PA swollen membranes, which are similar to the experimental situations, are shown in Fig. 4. The permeance of pure PA membrane is 721.5 L $m^{-2}h^{-1}$ bar^{-1} (LMHB) for the feed of pure water. Moreover, it is evident that the MMMs have higher permeance compared the pure PA membranes. This indicates that the MMMs have better permeability than the pure PA membranes. Comparing the permeance of Gr/PA MMMs to GO/PA MMMs, we could conclude that the Gr/PA MMMs have higher permeability. The transport mechanisms of two distinct MMMs will be discussed in section 3.3.

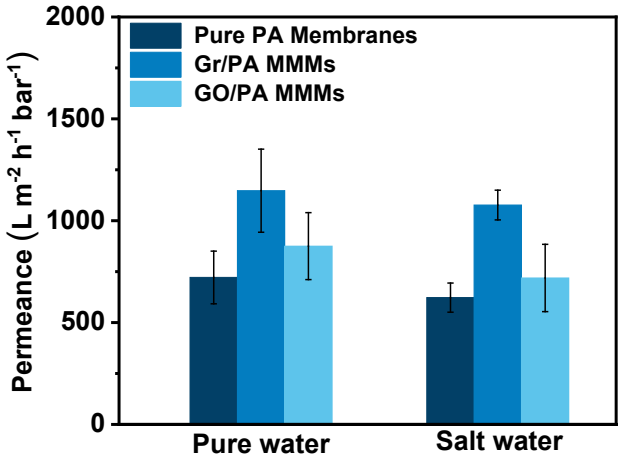

Fig. 4. Pure water and seawater permeances of swollen membranes. The error bar is calculated by five flux values which are calculated every 10 ns in the last 50 ns of the NEMD.

The permeances of seawater for three distinct membranes are slightly lower than those of pure water, respectively. The reduced permeance usually results from the osmotic pressure. As we observe that no ion can penetrate into the bulk region of membranes for all the three membranes in our 40-ns simulations, the estimated ion rejection is 100%. By comparing the seawater permeance of all three membranes, they exhibit the same trend with that of pure water permeances, indicating the transport performance will be nearly influenced by the feed condition. Hence, in the cases of non-swollen membranes that simulate the diffusion of fluid inside membranes, only pure water permeance is measured.

3.2. Molecular details of membranes during NEMDs

As revealed in the previous work [26,44,50,51], the permeance performance is usually determined by the physical and chemical structure of PA matrix, and therefore, we then pay attention to the structural and dynamic properties of membranes.

The densities of dry, non-swollen hydrated and swollen hydrated membranes are listed in Table 1. The water content of hydrated membranes (C_{water}), which is defined as $m_{water}/(m_{MMMs} + m_{water})$, are based on the density profiles in Fig. S2. The densities of all three dry membranes are almost the same, indicating the reliability of constructing the cross-linked membranes in this work. For the cases of swollen membranes, the water content of GO/PA MMMs is obviously higher, which is possible due to the better hydrophilicity of GO nanosheets. Higher water content will result in higher permeability of membranes [52], so the higher permeance of GO/PA membranes, compared to that of pure PA,

Table 1
Densities of dry, non-swollen hydrated and swollen hydrated membranes for all three membranes as well as their water content.

Membranes	ρ (g cm^{-3})/C_{water}		
	dry	non-swollen hydrated	swollen hydrated
Pure PA	1.061	1.028/23.2	0.994/27.0
Gr/PA	1.035	1.014/21.5	0.978/26.9
GO/PA	1.014	1.001/22.6	0.857/34.1

could be attributed to the higher water content.

It is surprising that the water content of Gr/PA MMMs is lower than that of pure PA membranes. However, the permeance of Gr/PA MMMs is much higher as shown in Fig. 4. As discussed in our previous work [51], the diffusion of water molecules plays an important role in the permeability of RO membranes. We calculate the mean square displacement (MSD) of PA atoms and water molecules inside the membranes (Fig. 5a). The MSD g(t) of polymer chains is shown as follows:

$$g(t) = [r_i(t) - r_i(0)]^2 \tag{3}$$

where r_i(t) and r_i(0) are the position of atom i at time t and 0, respectively.

It is obvious that the MSDs of PA atoms are much lower due to the highly cross-linked structure. Besides, the MSDs of water molecules are distinct for three membranes. The water MSD for Gr/PA MMMs rises more rapidly than other two, indicating the higher diffusive ability of Gr/PA MMMs. The water MSD for GO/PA MMMs rises slower than that of PA, possibly due to the hydrophilic nature of GO, which will definitely reduce the diffusion of water molecules [51,53].

In order to quantitatively characterize the diffusion of water molecules inside the PA membranes. The occupation time correlation function (R(t)) of water molecules inside the membranes are plotted in Fig. 5b, in which the sharper decrease indicates the higher diffusive ability. R(t) can be cast in the form

$$R(t) = \frac{1}{\Omega}\left[\frac{1}{t_0^{\max}}\sum_{t_0=1}^{t_0^{\max}}\frac{1}{N_{\text{occu}}}\sum_{i=1}^{N}\theta_i(t_0)\theta_i(t_0+t)\right] \tag{4}$$

where the function $\theta_i(t_0)$ is a function of a molecule i from the set of N molecules at time t. It equals 1, if molecule i is inside membranes at an initial time irrespective of its position at any other time, and 0 otherwise. Ω in the above equation is the normalization constant given by [54]

$$\Omega = \frac{1}{t_0^{\max}}\sum_{t_0=1}^{t_0^{\max}}\frac{1}{N_{\text{occu}}}\sum_{i=1}^{N}\theta_i(t_0)\theta_i(t_0) \tag{5}$$

where $t_0^{\max}$ is the total number of time origins considered for time averaging and N_{occu} is the number of molecules in the confined space averaged over all the time origins. It should be noted that the data from Fig. 5b are obtained from the simulations of non-swollen hydrated membranes, which will exclude the influence of various water content.

The R(t) drops more rapidly for the case of Gr/PA MMMs, indicating the higher diffusive ability of water molecules in such MMMs. Such a conclusion can be supported by our previous work that the hydrophobic membranes will have lower interior resistance when water molecules try to pass through them [51]. The GO/PA MMMs are more hydrophilic and consequently have lower diffusive ability for water molecules, so their R(t) drops slower even than that of pure PA membranes.

Since the diffusive ability and water content have opposite contributions to the permeability of membranes, it is required to quantitatively analyze the transport mechanism of MMMs, based on the data shown above.

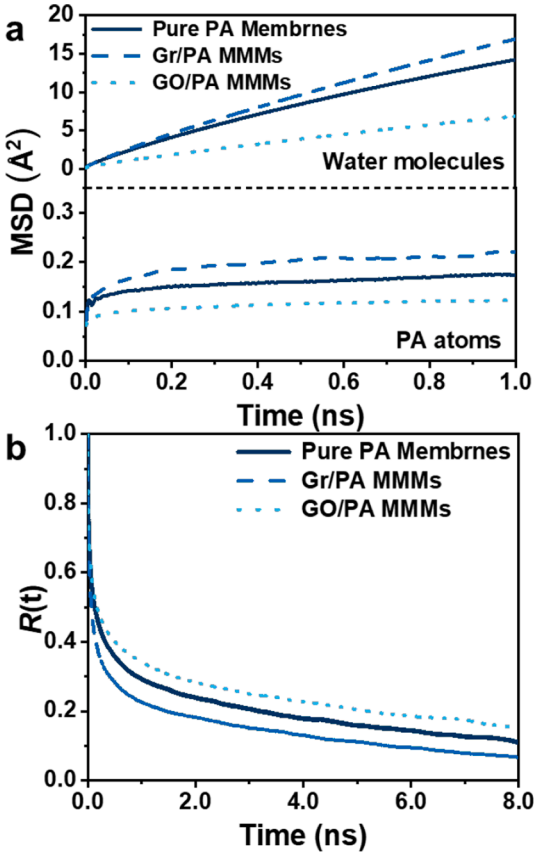

Fig. 5. (a)The mean square displacement (MSD) of PA atoms and water molecules inside the membranes (b) time correlation function (R(t)) of water molecules inside the membranes as a function of simulation time.

3.3. Analysis of the transport mechanism of MMMs

The classical model to describe water transport through PA RO membranes is the solution-diffusion (SD) model [55]. In SD model, the permeability (L) is described by,

$$L = \frac{DSV}{RTl} \tag{6}$$

where D is the diffusivity of water in the membrane, S is water solubility in the membrane, V is the partial molar volume of water, R is the gas constant, T is temperature and l is the thickness of the skin layer of the membrane. As the parameters of V, R, T, l are the same for all three membranes in this work, the contributions of diffusivity and solubility are focused on.

The diffusivity, known as the mass transport coefficient, is defined by the ratio of flux to the driving force [56]. The driving force is usually concentration gradient, but pressure drops in this work. As pressure drops for various cases in this work are all the same, we exclude it in the contribution. To calculate the flux of water molecules inside membranes, we turn to the average velocity of water molecules inside membranes. The average velocity of particles can be calculated by the ratio of membrane thickness to the residence time (τ) of water molecules inside membranes, which is obtained from the integration of R(t) in Fig. 5b.

$$D = \frac{l}{\tau} \tag{7}$$

The contribution of solubility is obtained from the data of water content (C_{water}).

$$S = \frac{C_{water}}{1 - C_{water}} \tag{8}$$

After obtaining diffusivity and solubility, we could relate the permeance enhancement (ε) of MMMs to the contribution of these two factors (shown in Fig. 6). When Gr nanosheets are added into PA membranes, the obtained MMMs have lower solubility but much higher diffusivity for water molecules. If the additive is replaced by GO nanosheets, the trend is completely different. The solubility is promoted evidently while the diffusivity will give a negative contribution. The calculated ε based on the contributions of solubility and diffusivity is listed in Table 2. For comparison, the ε from the permeance results of NEMD simulations is also listed in Table 2. Two sets of ε are in high accordance.

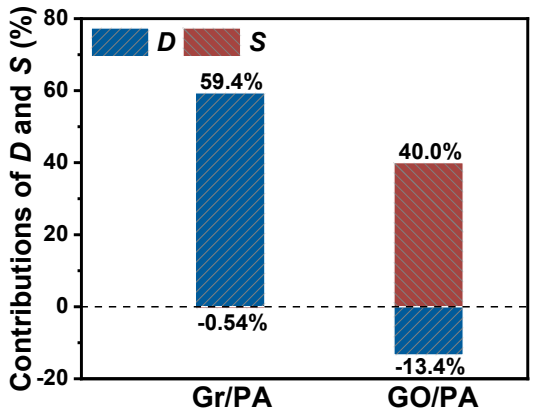

Fig. 6. The contributions of diffusivity (D) and solubility (S) of all three swollen membranes.

Table 2
The diffusivity and solubility of all three swollen membranes and the permeance enhancement for MMMs compared to pure PA membranes.

Membranes	Contributions		
	D_{MMM} (nm ns^{-1})	S_{MMM} (%)	ε (permeance/calculated)
Pure PA	2.72	37.0	
Gr/PA	4.34	36.8	59.0%/58.5%
GO/PA	2.36	51.8	21.3%/21.2%

Although the permeance enhancement of Gr/PA MMMs is higher than that of GO/PA MMMs, it is worth emphasizing that the Gr/PA MMMs are extremely prepared due to the poor dispersibility of Gr in MMMs, which will cause the problem of lacks and consequently result in the drop of desalination performance. It is interesting that the GO/PA MMMs exhibit the complete ion rejection even though their solubility is much higher. The highly cross-linked structure plays the most important role. The ε in our simulation (21.3) is quite close to the one (24.3) experimental work [57]. In that work, the ε reduces when the loading content of GO increase, possibly due to the large loading content resulting in the negative effect of diffusivity on permeance.

Since the adding of Gr and GO into PA matrix will certainly change the hydrophilicity of MMMs, the influence of hydrophilicity is also discussed. While hydrophilic membranes have better solubility, the diffusivity of water molecules inside them will be lower. There should be an optimized permeance due to opposite attribution of hydrophilicity on solubility and diffusivity. However, such optimized permeance is determined by the operation conditions because the solubility is also dependent on operation pressure [58]. If the loading content of nanosheets is reduced, the enhance degree of hydrophilicity or hydrophobicity while adding nanosheets will drops and the contributions of solubility and diffusivity enhancement will consequently decline. Therefore, the permeance will reduce close to that of pure PA membranes. Furthermore, the adjusting of oxidation degree of GO nanosheets can also attribute to the adjustment of hydrophilicity, and the same tendency will exhibit similar to the adjusting of loading content.

4. Conclusion

The MMMs draw much attention because they are promising candidates to replace the existing commercial pure aromatic PA RO membranes. Understanding the transport mechanism of water molecules through MMMs will help to design the RO membranes with promoted permeance. Highly cross-linked PA membranes, as well as Gr/PA and GO/PA MMMs are built up in atomic models. Following the hydration of these membranes, NEMD simulations are performed to observe the transport of water molecules through these membranes. The permeances of MMMs are evidently higher than those of pure PA membranes, while the Gr/PA MMMs exhibit the highest permeance. Due to the good compatibility of Gr or GO with PA matrix, there is no incompatible region observed in the MMMs. Therefore, the permeance enhancement might result from other reasons. After analyzing the water transport of interior regions of membranes, which is obtained from the models of non-swollen membranes, we conclude that the permeance enhancements of Gr/PA MMMs originate from the lower interior transport resistance due to the hydrophobic nature of Gr. In the case of GO/PA MMMs, the interior transport resistance is higher than that of pure PA membranes. However, the GO/PA MMMs also have advanced permeance compare to the pure PA membranes. This should be attributed to the higher water solubility of GO/PA MMMs. The contributions of solubility and diffusivity for MMMs are then quantitatively revealed. It should be noted that, to experimentally realize highest water permeation, efforts should be made to ensure the sufficient dispersion of Gr nanosheets and to avoid the dewetting of the MMMs. Moreover, the lower diffusivity from the hydrophilic GO nanosheets will reduce the permeance if the membrane thickness is much higher than that in this work. Therefore, there is an optimized permeance that is dependent on many factors, e.g. operation pressure drops, membrane thickness. We should take all factors into considerations when we design the RO membranes with expected performance.

CRediT authorship contribution statement

Guxu Wang: Conceptualization, Methodology, Software, Validation, Investigation, Formal analysis, Writing - original draft, Visualization. **Xin Zhang:** Investigation, Formal analysis. **Mingjie Wei:** Formal analysis, Writing - review & editing, Funding acquisition. **Yong Wang:** Formal analysis, Writing - review & editing, Supervision, Funding acquisition.

Declaration of Competing Interest

None.

Acknowledgments

Financial support from the National Key Research and Development Program of China (2017YFC0403902), the National Natural Science Foundation of China (21825803, 21921006), and the Jiangsu Natural Science Foundation (BK20190085) is acknowledged. We thank the High Performance Computing Center of Nanjing Tech University for supporting the computational resources. We are also grateful to the Program of Excellent Innovation Teams of Jiangsu Higher Education Institutions and the Project of Priority Academic Program Development of Jiangsu Higher Education Institutions (PAPD).

Appendix A. Supplementary material

Supplementary data to this article can be found online at https://doi.org/10.1016/j.seppur.2021.118818.

References

[1] X. Qu, J. Brame, Q. Li, P.J.J. Alvarez, Nanotechnology for a Safe and Sustainable Water Supply: Enabling Integrated Water Treatment and Reuse, Acc. Chem. Res. 46 (2013) 834–843.
[2] A. Al-Karaghouli, L.L. Kazmerski, Energy consumption and water production cost of conventional and renewable-energy-powered desalination processes, Renew. Sust. Energ. Rev. 24 (2013) 343–356.
[3] D. González, J. Amigo, F. Suárez, Membrane distillation: Perspectives for sustainable and improved desalination, Renew. Sustain. Energy Rev. 80 (2017) 238–259.
[4] M.A. Shannon, P.W. Bohn, M. Elimelech, J.G. Georgiadis, B.J. Marinas, A. M. Mayes, Science and technology for water purification in the coming decades, Nature 452 (2008) 301–310.

[5] M. Qin, A. Deshmukh, R. Epsztein, S.K. Patel, O.M. Owoseni, W.S. Walker, M. Elimelech, Comparison of energy consumption in desalination by capacitive deionization and reverse osmosis, Desalination 455 (2019) 100–114.
[6] Z. Jiang, S. Karan, A.G. Livingston, Water Transport through Ultrathin Polyamide Nanofilms Used for Reverse Osmosis, Adv. Mater. 30 (2018) 1705973.
[7] Z. Tan, S. Chen, X. Peng, L. Zhang, C. Gao, Polyamide membranes with nanoscale Turing structures for water purification, Science 360 (2018) 518–521.
[8] Z. Wang, Z. Wang, S. Lin, H. Jin, S. Gao, Y. Zhu, J. Jin, Nanoparticle-templated nanofiltration membranes for ultrahigh performance desalination, Nat. Commun. 9 (2018) 2004.
[9] B.-H. Jeong, E.M.V. Hoek, Y. Yan, A. Subramani, X. Huang, G. Hurwitz, A.K. Ghosh, A. Jawor, Interfacial polymerization of thin film nanocomposites: A new concept for reverse osmosis membranes, J. Membr. Sci. 294 (2007) 1–7.
[10] D.L. Zhao, S. Japip, Y. Zhang, M. Weber, C. Maletzko, T.-S. Chung, Emerging thin-film nanocomposite (TFN) membranes for reverse osmosis: A review, Water Res. 173 (2020), 115557.
[11] P.H.C. Jensen, DK), Keller, Danielle (Odense, DK), Nielsen, Claus Hélix (Taastrup, DK), Membrane for filtering of water, in, Aquaporin A/S, Copehhagen N, DK), United States, 2010.
[12] G. Zhang, J. Zhang, P. Lv, J. Sun, P. Zhao, L. Yang, Modifying thin film composite membrane with zeolitic imidazolate framework-8@polydopamine for enhanced antifouling property, Chemosphere 248 (2020), 125956.
[13] J. Park, W. Choi, S.H. Kim, B.H. Chun, J. Bang, K.B. Lee, Enhancement of Chlorine Resistance in Carbon Nanotube Based Nanocomposite Reverse Osmosis Membranes, Desalin. Water Treat. 15 (2010) 198–204.
[14] W.-F. Chan, H.-Y. Chen, A. Surapathi, M.G. Taylor, X. Shao, E. Marand, J. K. Johnson, Zwitterion Functionalized Carbon Nanotube/Polyamide Nanocomposite Membranes for Water Desalination, ACS Nano 7 (2013) 5308–5319.
[15] J.n. Shen, C.c. Yu, H.m. Ruan, C.j. Gao, B. Van der Bruggen, Preparation and characterization of thin-film nanocomposite membranes embedded with poly (methyl methacrylate) hydrophobic modified multiwalled carbon nanotubes by interfacial polymerization, J. Membr. Sci., 442 (2013) 18-26.
[16] H.D. Lee, H.W. Kim, Y.H. Cho, H.B. Park, Experimental Evidence of Rapid Water Transport through Carbon Nanotubes Embedded in Polymeric Desalination Membranes, Small 10 (2014) 2653–2660.
[17] S.-Y. Kwak, S.H. Kim, S.S. Kim, Hybrid Organic/Inorganic Reverse Osmosis (RO) Membrane for Bactericidal Anti-Fouling. 1. Preparation and Characterization of TiO2 Nanoparticle Self-Assembled Aromatic Polyamide Thin-Film-Composite (TFC) Membrane, Environ. Sci. Technol. 35 (2001) 2388–2394.
[18] W. Gai, Y. Zhang, Q. Zhao, T.-S. Chung, Highly permeable thin film composite hollow fiber membranes for brackish water desalination by incorporating amino functionalized carbon quantum dots and hypochlorite treatment, J. Membr. Sci. 620 (2021), 118952.
[19] W. Gai, D.L. Zhao, T.-S. Chung, Thin film nanocomposite hollow fiber membranes comprising Na+-functionalized carbon quantum dots for brackish water desalination, Water Res. 154 (2019) 54–61.
[20] H.J. Kim, K. Choi, Y. Baek, D.-G. Kim, J. Shim, J. Yoon, J.-C. Lee, High-Performance Reverse Osmosis CNT/Polyamide Nanocomposite Membrane by Controlled Interfacial Interactions, ACS Appl. Mater. Interfaces 6 (2014) 2819–2829.
[21] C. Wang, Z. Li, J. Chen, Z. Li, Y. Yin, L. Cao, Y. Zhong, H. Wu, Covalent organic framework modified polyamide nanofiltration membrane with enhanced performance for desalination, J. Membr. Sci. 523 (2017) 273–281.
[22] R.R. Gonzales, M.J. Park, T.-H. Bae, Y. Yang, A. Abdel-Wahab, S. Phuntsho, H. K. Shon, Melamine-based covalent organic framework-incorporated thin film nanocomposite membrane for enhanced osmotic power generation, Desalination 459 (2019) 10–19.
[23] H.-R. Chae, J. Lee, C.-H. Lee, I.-C. Kim, P.-K. Park, Graphene oxide-embedded thin-film composite reverse osmosis membrane with high flux, anti-biofouling, and chlorine resistance, J. Membr. Sci. 483 (2015) 128–135.
[24] L. Bai, Y. Liu, A. Ding, N. Ren, G. Li, H. Liang, Fabrication and characterization of thin-film composite (TFC) nanofiltration membranes incorporated with cellulose nanocrystals (CNCs) for enhanced desalination performance and dye removal, Chem. Eng. J. 358 (2019) 1519–1528.
[25] Y. Li, S. Yang, K. Zhang, B. Van der Bruggen, Thin film nanocomposite reverse osmosis membrane modified by two dimensional laminar MoS2 with improved desalination performance and fouling-resistant characteristics, Desalination 454 (2019) 48–58.
[26] Y. Song, M. Wei, F. Xu, Y. Wang, Transport mechanism of water molecules passing through polyamide/COF mixed matrix membranes, Phys. Chem. Chem. Phys. 21 (2019) 26591–26597.
[27] M. Ding, A. Szymczyk, F. Goujon, A. Soldera, A. Ghoufi, Structure and dynamics of water confined in a polyamide reverse-osmosis membrane: A molecular-simulation study, J. Membr. Sci. 458 (2014) 236–244.
[28] V. Kolev, V. Freger, Hydration, porosity and water dynamics in the polyamide layer of reverse osmosis membranes: A molecular dynamics study, Polymer 55 (2014) 1420–1426.
[29] E. Harder, D.E. Walters, Y.D. Bodnar, R.S. Faibish, B. Roux, Molecular Dynamics Study of a Polymeric Reverse Osmosis Membrane, J. Phys. Chem. B 113 (2009) 10177–10182.
[30] Z.E. Hughes, J.D. Gale, A computational investigation of the properties of a reverse osmosis membrane, J. Mater. Chem. 20 (2010) 7788–7799.
[31] C.Y. Tang, Y.-N. Kwon, J.O. Leckie, Probing the nano- and micro-scales of reverse osmosis membranes—A comprehensive characterization of physiochemical properties of uncoated and coated membranes by XPS, TEM, ATR-FTIR, and streaming potential measurements, J. Membr. Sci. 287 (2007) 146–156.
[32] O. Coronell, B.J. Mariñas, D.G. Cahill, Depth Heterogeneity of Fully Aromatic Polyamide Active Layers in Reverse Osmosis and Nanofiltration Membranes, Environ. Sci. Technol. 45 (2011) 4513–4520.
[33] V.T. Do, C.Y. Tang, M. Reinhard, J.O. Leckie, Degradation of Polyamide Nanofiltration and Reverse Osmosis Membranes by Hypochlorite, Environ. Sci. Technol. 46 (2012) 852–859.
[34] B. Mi, O. Coronell, B.J. Mariñas, F. Watanabe, D.G. Cahill, I. Petrov, Physico-chemical characterization of NF/RO membrane active layers by Rutherford backscattering spectrometry, J. Membr. Sci. 282 (2006) 71–81.
[35] J. Liu, X. Kong, J. Jiang, Solvent nanofiltration through polybenzimidazole membranes: Unravelling the role of pore size from molecular simulations, J. Membr. Sci. 564 (2018) 782–787.
[36] A. Lerf, H. He, M. Forster, J. Klinowski, Structure of Graphite Oxide Revisited, J. Phys. Chem. B 102 (1998) 4477–4482.
[37] N.V. Medhekar, A. Ramasubramaniam, R.S. Ruoff, V.B. Shenoy, Hydrogen Bond Networks in Graphene Oxide Composite Paper: Structure and Mechanical Properties, ACS Nano 4 (2010) 2300–2306.
[38] D.R. Dreyer, S. Park, C.W. Bielawski, R.S. Ruoff, The chemistry of graphene oxide, Chem. Soc. Rev. 39 (2010) 228–240.
[39] K.A. Mkhoyan, A.W. Contryman, J. Silcox, D.A. Stewart, G. Eda, C. Mattevi, S. Miller, M. Chhowalla, Atomic and Electronic Structure of Graphene-Oxide, Nano Lett. 9 (2009) 1058–1063.
[40] R. Raj, S.C. Maroo, E.N. Wang, Wettability of Graphene, Nano Lett. 13 (2013) 1509–1515.
[41] M. Heiranian, A.B. Farimani, N.R. Aluru, Water desalination with a single-layer MoS2 nanopore, Nat. Commun. 6 (2015).
[42] D. Cohen-Tanugi, J.C. Grossman, Water desalination across nanoporous graphene, Nano Lett. 12 (2012) 3602–3608.
[43] K. Zhang, Z. He, K.M. Gupta, J. Jiang, Computational design of 2D functional covalent-organic framework membranes for water desalination, Environ. Sci. Water Res. Technol. 3 (2017) 735–743.
[44] M. Shen, S. Keten, R.M. Lueptow, Dynamics of water and solute transport in polymeric reverse osmosis membranes via molecular dynamics simulations, J. Membr. Sci. 506 (2016) 95–108.
[45] P.G. Kusalik, I.M. Svishchev, The Spatial Structure in Liquid Water, Science 265 (1994) 1219–1221.
[46] J. Wang, R.M. Wolf, J.W. Caldwell, P.A. Kollman, D.A. Case, Development and testing of a general amber force field, J. Comput. Chem. 25 (2004) 1157–1174.
[47] M. Ding, A. Szymczyk, A. Ghoufi, Hydration of a polyamide reverse-osmosis membrane, J. Membr. Sci. 501 (2016) 248–253.
[48] W.L. Jorgensen, D.S. Maxwell, J. TiradoRives, Development and testing of the OPLS all-atom force field on conformational energetics and properties of organic liquids, J. Am. Chem. Soc. 118 (1996) 11225–11236.
[49] S. Plimpton, Fast parallel algorithms for short-range molecular dynamics, J. Comput. Phys. 117 (1995) 1–19.
[50] M. Ding, A. Szymczyk, A. Ghoufi, On the structure and rejection of ions by a polyamide membrane in pressure-driven molecular dynamics simulations, Desalination 368 (2015) 76–80.
[51] Y. Song, M. Wei, F. Xu, Y. Wang, Molecular simulations of water transport resistance in polyamide RO membranes: Interfacial and interior contributions, Engineering 6 (2020) 577–584.
[52] M.F. Jimenez-Solomon, Q. Song, K.E. Jelfs, M. Munoz-Ibanez, A.G. Livingston, Polymer nanofilms with enhanced microporosity by interfacial polymerization, Nat. Mater. 15 (2016) 760.
[53] F. Xu, Y. Song, M. Wei, Y. Wang, Water flow through interlayer channels of two-dimensional materials with various hydrophilicities, J. Phys. Chem. C 122 (2018) 15772–15779.
[54] N. Choudhury, B.M. Pettitt, Dynamics of Water Trapped between Hydrophobic Solutes, J. Phys. Chem. B 109 (2005) 6422–6429.
[55] A.F. Ismail, T. Matsuura, Progress in transport theory and characterization method of Reverse Osmosis (RO) membrane in past fifty years, Desalination 434 (2018) 2–11.
[56] R.B. Bird, W.E. Stewart, E.N. Lightfoot, Transport phenomena, John Wiley & Sons, 2006.
[57] S. Xia, L. Yao, Y. Zhao, N. Li, Y. Zheng, Preparation of graphene oxide modified polyamide thin film composite membranes with improved hydrophilicity for natural organic matter removal, Chem. Eng. J. 280 (2015) 720–727.
[58] F. Xu, M. Wei, X. Zhang, Y. Song, W. Zhou, Y. Wang, How pore hydrophilicity influences water permeability? Research 2019 (2019) 10.